Mechanisms in the autogenous mill and their mathematical representation

by G. G. STANLEY*, B.Sc. (Eng.) (Wits.), M.E. (Queensland), Ph.D., (Fellow)

SYNOPSIS

The special characteristics of the autogenous mill are stated, and a suitable type of model for the mill is presented. Details of the test plant and experimental techniques for obtaining the data for model development are next given, followed by a discussion of the methods developed for the computation of the model parameters, namely the appearance matrix, the abrasion and crushing breakage-rate functions, and the discharge-rate function. Examples of results obtained with the model are given, and finally there is a brief account of confirmatory work on a full-scale autogeneous mill.

SAMEVATTING

Die spesiale eienskappe van die outogene meul word genaam en 'n geskikte tipe model vir die meul word voorgestel. Vervolgens word besonderhede verstrek van die toetsaanleg en eksperimentele tegnieke om data vir die ontwikkeling van die model te bekom en dit word gevolg deur 'n bespreking van die metodes wat ontwikkel is vir die berekening van die modelparameters, naamlik die voorkomsmatriks, die funksies vir die skuur- en vergruisingsbreektempo en die ontlandingstempofunksie. Daar word voorbeelde gegee van die resultate wat met die model verkry is en ten slotte is daar 'n kort verslag oor bevestigende werk by 'n volskaalse outogene meul.

INTRODUCTION

Over the past twenty or thirty years, mathematical modelling of ball and rod mills has been widely investigated, and reasonably satisfactory models are now available. The autogenous mill has, however, received very little attention in this respect, and in view of the increasing importance of this type of mill, the Julius Kruttschnitt Mineral Research Centre in the Department of Mining and Metallurgical Engineering, University of Queensland, in 1970 commenced a programme of research into mathematical modelling of the autogenous mill. This paper reports the work of the author on this programme from its inception until the end of 1973.

THE AUTOGENOUS MILL FROM THE MATHEMATICAL MODELLING VIEWPOINT

Autogenous Milling Defined

As used in this study, the term *autogenous milling* means a process in which the size of the constituent pieces of a supply of rock is reduced in a tumbling mill purely by the interaction of the pieces, or by the interaction of the pieces with the mill shell, no other grinding medium being employed. The definition thus covers both 'run-of-mine' and 'pebble' milling, the only difference from the mathematical modelling viewpoint being that the feed to the first has a continuous, and the second a non-continuous, size distribution.

Special Characteristics of the Autogenous Mill

Autogenous milling differs fundamentally from non-autogenous milling in two respects.

(1) Size reduction occurs by two main modes, namely the detachment of material from the surface of larger particles (referred to as 'abrasion') on the one hand, and disintegration of smaller particles due to the propagation of crack networks through them (called 'crushing') on the other. Abrasion and crushing breakage overlap on the size scale. This contrasts with non-autogenous milling, in which only crushing breakage, however caused, is regarded as significant.

(2) The grinding parameters of the autogenous mill load are not independent of the mill feed; the load is continually generated from the feed, and its parameters therefore depend directly on those of the feed.

These two charactersistics must be specifically included in the model of the autogenous mill.

THE PERFECT MIXING MODEL

Because of the importance of the load in autogenous milling, the type of model adopted is basically the discretized mass balance of the size fractions in the load, and is known as the 'perfect mixing model' because of its assumption of this condition within the segment considered. Its theory has been developed by Whiten[1].

In matrix notation, the perfect mixing model is written

$$\frac{d\underline{s}}{dt}=(AR-R)\underline{s}+\underline{f}-\underline{p}, \quad \ldots . (1)$$

where $\underline{s}$ is a vector of the mass contents of the segment in successive size fractions,

$\underline{f}$ is a vector of the mass flowrates of the successive fractions of feed to the segment,

$\underline{p}$ is a vector of the mass flowrates of the successive fractions of the discharge from the segment,

R is a diagonal matrix giving the breakage rate of each component of $\underline{s}$, and

A is a lower triangular matrix (the appearance matrix) containing in each column the breakage function for the corresponding size fraction. If the breakage functions are identical, A becomes a step matrix.

The relationship between contents and product is

$$\underline{p}=D.\underline{s},$$

where D (the discharge matrix) is a diagonal matrix giving the discharge rates of each component of $\underline{s}$.

Thus,

$$\frac{d\underline{s}}{dt}=(AR-R-D)\,\underline{s}+\underline{f} \qquad (2)$$

and, for the steady-state condition,

$$(AR-R-D).\underline{s}+\underline{f}=0. \quad \ldots . (3)$$

If A is known or assumed, and

*National Institute for Metallurgy, Johannesburg.

f, s, and p are known, both R and D can be computed. If s, the mill contents, is not known, then R and D cannot be separated; however, a combined parameter, such as DR^{-1}, can be calculated if f and p are known.

Lees[2] has shown that even a large 'square mill' (3,2m in diameter by 3,06m) can be adequately represented by a single perfectly-mixed segment and, because of this and the high ratio of diameter to length in the author's experimental mill, the same simplification was adopted in the work reported here.

EXPERIMENTAL DETAILS

The experimental work on which the model of the autogenous mill was based was aimed essentially at determining the relationships between feed size, rate, and density on the one hand and parameters A, R, and D of the perfect-mixing model on the other. The test programme therefore comprised a series of tests in which the feed characteristics mentioned were systematically varied and the effects on A, R, and D determined.

Special Feeding Technique for Constant Size Distribution

The problem of feeding the mill consistently, both with respect to rate and size distribution, was solved by segregation of the test ore parcel into eight size fractions and feeding them individually. The four plus 76mm fractions were fed lump by lump at time intervals calculated from average lump weight in each fraction to give preselected size distributions. Timing of the additions was achieved by passing a paper strip chart, previously marked at calculated intervals, at known speed under a fixed index, and feeding a lump as each successive mark reached the index. A separate series of marks was made for each of the four size fractions (Plate I).

TABLE I

SIZE DISTRIBUTION, COBAR EASTERN ORE

Size range, μm		Differential percentage
	+304800	0,1
−304800	+254000	0,1
−254000	+203200	1,1
−203200	+152400	4,4
−152400	+101600	8,7
−101600	+76200	5,7
−76200	+50800	9,7
−50800	+25400	20,7
−25400	+12700	15,9
−12700	+9525	4,8
−9525	+6350	4,3
−6350	+4763	3,5
−4763	+1676	5,8
−1676	+1204	1,5
−1204	+853	1,1
−853	+600	1,1
−600	+422	0,9
−422	+295	0,9
−295	+211	0,9
−211	+152	0,9
−152	+104	1,3
−104	+76	1,0
−76	+53	0,9
−53		4,7
		100,0

The four minus 76mm fractions were also fed independently, the necessary weights of the fractions for five minutes' mill feed at the desired size distribution being preweighed into each of a number of sacks. One such sack was emptied each 5 minutes onto the feed belt and spread out to give a continuous feed over that time interval.

The overall size distribution of the run-of-mine ore is given in Table I.

The effect of mill parameters such as size and speed was not investigated.

The experimental plant was the pilot run-of-mine autogenous milling installation of Cobar Mines Pty Ltd, Cobar, New South Wales, consisting of a grate-discharge Hardinge 'Cascade' mill (1,6m in diameter by 0,3m long) running at 70 per cent of critical speed, usually in closed circuit with a 7,5cm hydrocyclone. As described later, some open-circuit tests were run with 'synthetic' circulating loads composed of material from the cyclone underflows of the main Cobar autogenous milling plant. The mill was fed by a 3m-long conveyor belt running at 0,35m per minute; circuit feed was manually loaded onto this belt, as already described. Fig. 1 is the flowsheet and Plate II a general view of the installation.

For the testwork, a special 100-tonne parcel of Cobar Eastern ore was hoisted and delivered to the pilot plant. The ore consisted mainly of silicified slates and cherts containing finely disseminated chalcopyrite and other sulphides. Occasional massive sulphide was encountered, and stringers of quartz in the slaty material were frequently evident. In spite of the slaty nature of the ore, however, there was no marked tendency to breakage in the mill along the bedding planes, presumably because of the silicification. The specific gravity of the ore was about 3,1.

Synthetic Circulating Loads

In a normal mill-classifier closed circuit, a change in the size distribution of the classifier feed changes the underflow sizing, and hence the mill-feed sizing. This makes it very difficult to isolate the effect of a change in milling conditions such as discharge pulp density or circulating load ratios. The effects of these two operating variables were therefore

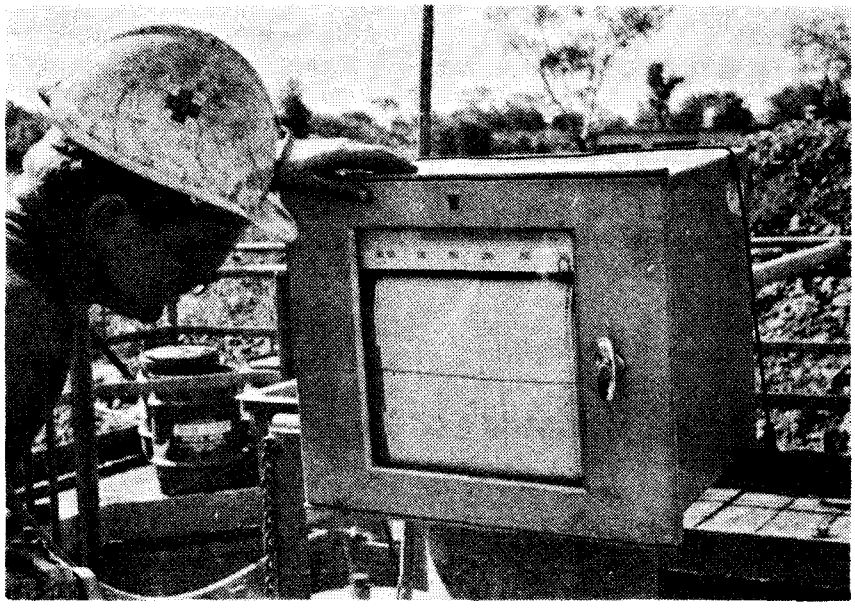

Plate I—The strip recorder, adapted to pebble feed control, which was located adjacent to the mill feed hopper

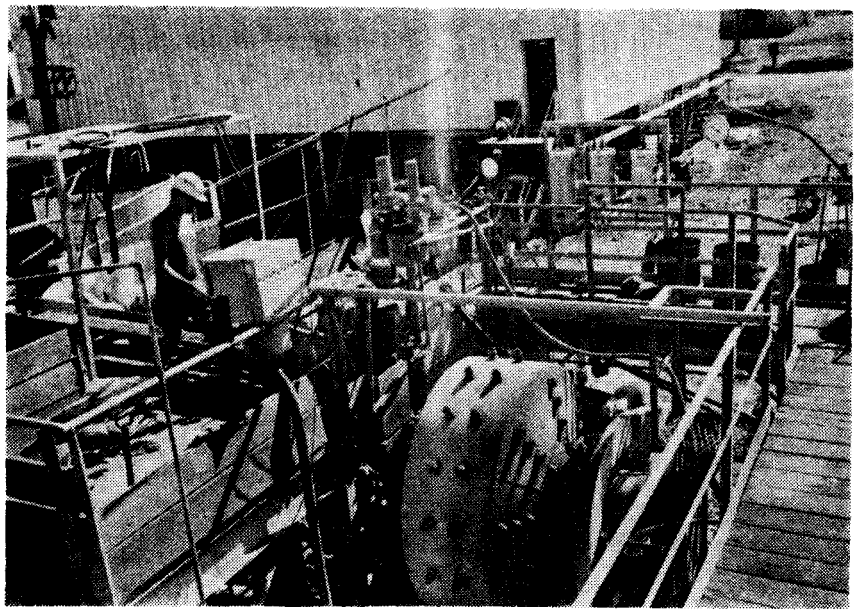

Plate II—A general view of the installation

determined by means of open-circuit tests, using a 'synthetic' circulating load of constant size distribution that was fed dry in various pre-determined ratios to the normal circuit feed.

Test Method

Wherever possible, tests started with mill loads made up of material from previous loads, the object being to reduce the time to reach equilibrium, although the closed-circuit tests were in any case run for 8 hours, this being an adequate time for the attainment of equilibrium as indicated by a preliminary series of tests. Starting load weights, size distributions, and water contents were made up to an estimate, from previous tests, of the load that would be generated in the test to be run.

Power consumption and pulp densities were recorded half-hourly during the course of each test run. At she conclusion of each run, the pulp streams were sampled for size analysis, and the mass flowrate of the cyclone underflow was determined by directing the stream into a container for a measured time. Mill inlet water, cyclone underflow, and new feed were cut off simultaneously and the mill stopped; the mill contents were then unloaded through the feed trunnion into specially made watertight trolleys, weighed wet, and spread on plastic sheets to sun-dry. Wet loads weighed about 1000kg, with about 6 per cent moisture content. The load discharging and weighing arrangements are shown in Plate III. Representative numbers of pieces from each of the load fractions down to 9,5mm were counted and weighed. Average weights per piece for both new feed and load fractions are plotted against size in Fig. 2, in which it can be seen that both products conform to the relationship

$$\text{Weight of pebble (g)} = \frac{d^3}{496{,}53}, \quad (4)$$

where d=square-mesh size in millimetres.

Size distributions from 4762μm downwards were determined on a full BSS series of screens. Above 4762μm, the screens used were not in $\sqrt{2}$ relationship, but the distributions determined were computer-transposed onto a $\sqrt{2}$ series conformable with the BSS system.

COMPUTATION OF BREAKAGE RATES

Breakage Functions for Crushing and Abrasion

Before breakage rates for the various size fractions in each of the tests could be computed, a breakage-function matrix had to be set up. It is in this matrix that the simultaneous abrasion and crushing breakage features of the autogenous mill are included.

The matrix is of lower triangular form, containing in successive columns the breakage function for the corresponding size fraction. Thus, for the autogenous mill, the matrix will contain a function or functions representing abrasion breakage in the coarse sizes and another function describing crushing breakage in the finer sizes, with a transition zone between the two.

In the work reported here, abrasion breakage was described by a largely intuitive function based on a consideration of the nature of abrasion breakage. The latter has been defined as size reduction by the superficial detachment of relatively

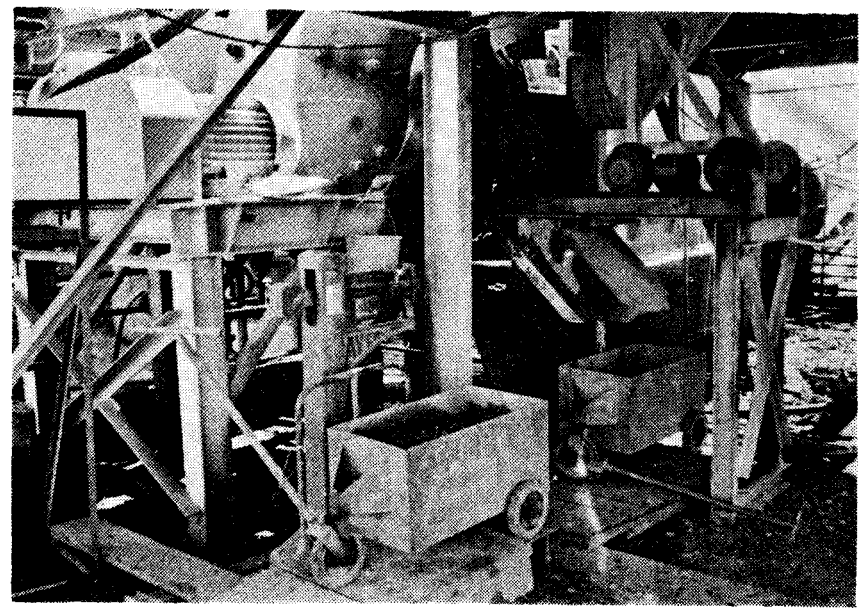

Plate III—Arrangements for the discharge and weighing of the load

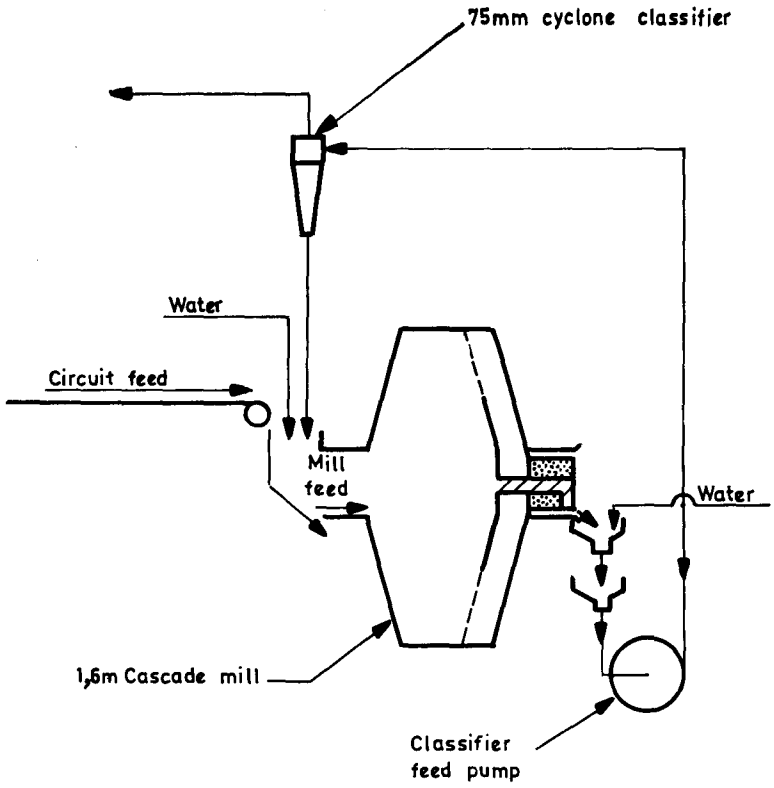

Fig. 1—The flowsheet of the experimental milling circuit

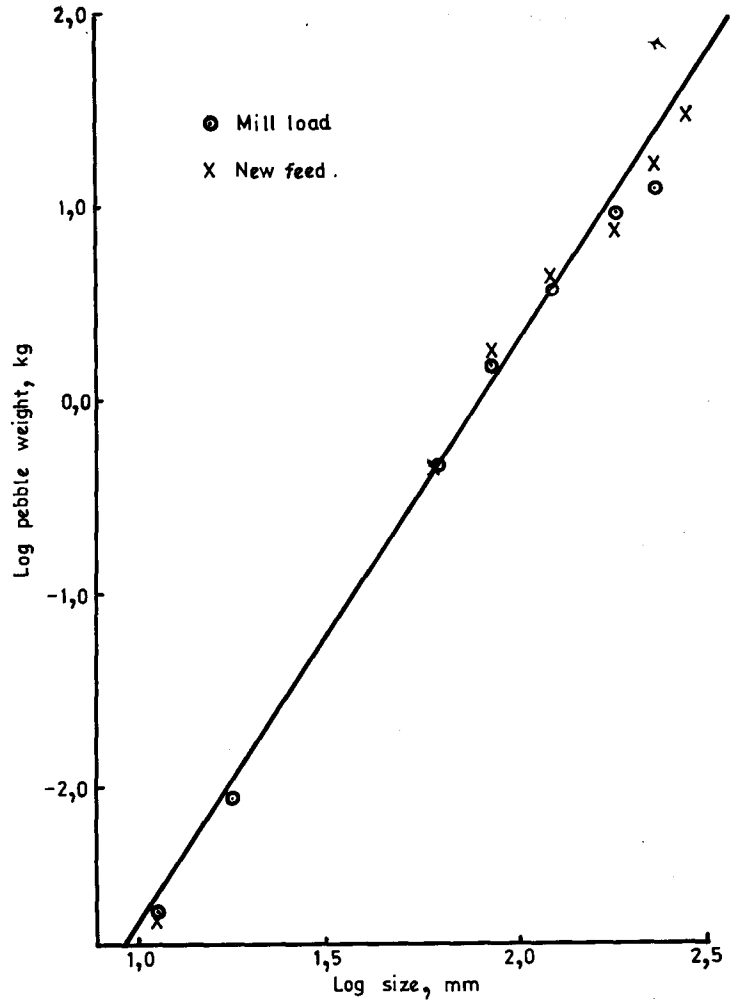

Fig. 2—Average mass of pebble *versus* size

fine material from the surface of larger pieces; it results in the slow 'whittling away' of a central core with the concomitant production of an increasing quantity of fine detritus. Thus, when pieces evenlv distributed over a single size fraction are subjected to an abrasion breakage 'event', all the pieces will be slightly reduced in size, some near the lower limit of the fraction will pass into the next smaller fraction, and the material abraded from the original pieces will report to a number of size ranges somewhat further down the size scale.

From a consideration of the relative mean weights of particles in successive $\sqrt{2}$ size fractions, a worker at the Kruttschnitt Centre, P. Wickham, postulated that, if the particles in a single size interval lose a proportion x of their weight as the result of an abrasion breakage event, then $0{,}354x$ (i.e. $(1/\sqrt{2})^3 x$) will appear in the next smaller $\sqrt{2}$ interval, and the remaining $0{,}646x$ will form the detritus, which is spread over a number of considerably smaller size intervals[3]. This postulate, with $x=0{,}01$, was adopted for the present work, and the function used to describe abrasion breakage is given in Table II. The detritus was arbitrarily given a Rosin-Rämmler distribution, and the gap of five size intervals between the abraded cores and the detritus was also purely arbitrary.

TABLE II

ABRASION-BREAKAGE FUNCTION, $x=0{,}01$

Number of size fraction	Proportion appearing in fraction after breakage
1	0,9900
2	0,0035
3	0,0000
4	0,0000
5	0,0000
6	0,0000
7	0,0000
8	0,0007
9	0,0012
10	0,0011
11	0,0009
12	0,0007
13	0,0005
14	0,0004
15	0,0003
16	0,0002
17	0,0002
18	0,0001
19	0,0000
20	0,0000
21	0,0000
22	0,0000
23	0,0000
24	0,0000
25	0,0000

Abrasion breakage	Transition zone						Crushing breakage
a 0 0 . .	0	0	0	0	0	0	. . 0 0
b a 0 . .	0	0	0	0	0	0	. . 0 0
c b a . .	0	0	0	0	0	0	. . 0 0
d c b . .	0	0	0	0	0	0	. . 0 0
e d c . .	0	0	0	0	0	0	. . 0 0
f e d . .	0	0	0	0	0	0	. . 0 0
g f e . .	$a_1a+(1-a_1)p$	0	0	0	0	0	. . 0 0
h g f . .	$a_1b+(1-a_1)q$	$a_2a+(1-a_2)p$	0	0	0	0	. . 0 0
. h g . .	$a_1c+(1-a_1)r$	$a_2b+(1-a_2)q$	$a_3a+(1-a_3)p$	0	0	0	. . 0 0
. . h . .	$a_1d+(1-a_1)s$	$a_2c+(1-a_2)r$	$a_3b+(1-a_3)q$	$a_4a+(1-a_4)p$	0	0	. . 0 0
. . . . .	$a_1e+(1-a_1)t$	$a_2d+(1-a_2)s$	$a_3c+(1-a_3)r$	$a_4b+(1-a_4)q$	$a_5a+(1-a_5)p$	0	. . 0 0
. . . . .	$a_1f+(1-a_1)u$	$a_2e+(1-a_2)t$	$a_3d+(1-a_3)s$	$a_4c+(1-a_4)r$	$a_5b+(1-a_5)q$	$a_6a+(1-a_6)p$	. . 0 0
. . . . .	.	$a_2f+(1-a_2)u$	$a_3e+(1-a_3)t$	$a_4d+(1-a_4)s$	$a_5c+(1-a_5)r$	$a_6b+(1-a_6)q$	. . 0 0
. . . . .	.	.	$a_3f+(1-a_3)u$	$a_4e+(1-a_4)t$	$a_5d+(1-a_5)s$	$a_6c+(1-a_6)r$	. . 0 0
. . . . .	.	.	.	$a_4f+(1-a_4)u$	$a_5e+(1-a_5)t$	$a_6d+(1-a_6)s$	. . p 0
. . . . .	.	.	.	.	$a_5f+(1-a_5)u$	$a_6e+(1-a_6)t$	. . q p
. . . . .	.	.	.	.	.	$a_6f+(1-a_6)u$	. . r q
. . . . .	.	.	.	.	.	.	s r

Fig. 3—The general scheme of the three-part matrix

To describe crushing breakage, a modification of the Rosin-Rämmler distribution proposed by Broadbent and Callcott[4] and further modified by Whiten was used in the work on the autogenous mill:

$$B(x,y)=\frac{1-e^{-(x/y)^p}}{1-e^{-1}},$$

where $B(x,y)$ is the proportion of particles originally of size y that are smaller than size x after breakage. The addition of the index p is Whiten's modification and, where p is greater than 1, the effect is to concentrate the products of breakage nearer the parent size than when p is equal to 1. In the present work, the best value of p was found to be 2, and the resulting breakage function is given in Table III.

TABLE III

CRUSHING-BREAKAGE FUNCTION

Number of size fraction	Proportion appearing in fraction after breakage
1	0,1979
2	0,3310
3	0,2147
4	0,1226
5	0,0654
6	0,0338
7	0,0172
8	0,0087
9	0,0043
10	0,0022
11	0,0011
12	0,0005
13	0,0003
14	0,0001
15	0,0001
16	0,0000
17	0,0000
18	0,0000
19	0,0000
20	0,0000
21	0,0000
22	0,0000
23	0,0000
24	0,0000
25	0,0000

The same modified Rosin-Rämmler crushing breakage function was assumed to hold regardless of the initial particle size, so that the crushing breakage portion of the breakage matrix became a 'step' matrix. Several workers have pointed out that this assumption is not strictly true[5,6], but it is sufficiently accurate for the present purpose, as is the very arbitrary abrasion break-

TABLE IV

EQUATIONS FOR ABRASION LIMIT

Calculation size (first $\sqrt{2}$ size retaining at least 2% of mill feed), μm	Equation for abrasion limit, μm (x = percentage of mill feed retained on calculation size)
151712	$\log_{10}$ abrasion limit = $(2,45 + 0,32x).\ x^{\frac{1}{1,3+x}}$
107296	$\log_{10}$ abrasion limit = $(2,45 + 0,12x).\ x^{\frac{1}{1,3+x}}$
75856	$\log_{10}$ abrasion limit = $(2,45 + 0,09x).\ x^{\frac{1}{1,3+x}}$
53648	$\log_{10}$ abrasion limit = $(2,45 + 0,06x).\ x^{\frac{1}{1,3+x}}$

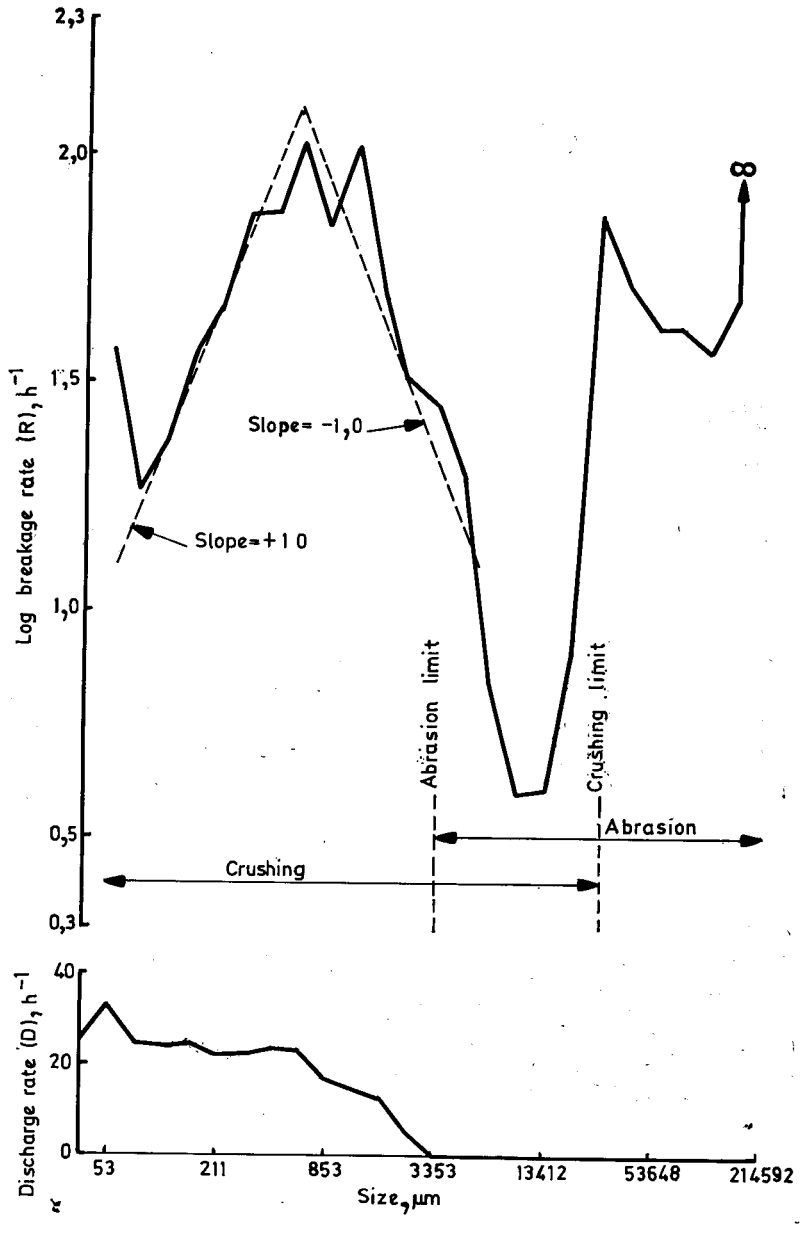

Fig. 4—Typical breakage-rate and discharge-rate functions

age function adopted. As Lynch and Moore[7] have stated, the general form of the predicted size distribution for the mill discharge is more important than its precise details.

The Abrasion-to-Crushing Transition

Two final parameters need to be known before the complete breakage-function matrix can be set up; namely, the upper and lower limits of the transition zone between abrasion and crushing breakage. The upper limit, i.e. the size above which no crushing breakage occurs, has been named the crushing limit; similarly, the lower limit, the size below which no abrasion breakage occurs, has been designated the abrasion limit.

The crushing and abrasion limits in each of the test runs were determined by visual examination of the size fractions in the load. By such examination, it was possible to fix the size interval in which the sharp edges and conchoidal faces characteristic of crushing breakage first appeared to any significant extent among the smooth fragments generated by abrasion. The upper size of this interval was taken to be the crushing limit. Through successively finer fractions, it was noted that the proportion of fragments resulting from crushing steadily increased at the expense of those resulting from abrasion, until the latter disappeared completely. The upper size of the first interval to contain no abraded fragments was taken as the abrasion limit. Generally, the transition from all-abrasion to all-crushing occupied six $\sqrt{2}$ size intervals.

It was found that the crushing limit could be related to the concentrations of any of the four coarsest $\sqrt{2}$ size fractions in the mill feed (i.e. new feed plus classifier underflow), provided that such a fraction constituted at least 2 per cent by weight of the mill feed. The relationships obtained are given in Table IV. It was found, however, that they became unreliable at relatively high concentrations of the respective size fractions, and therefore an upper limit of 26824μm was set on computed crushing limits. The abrasion limit was taken as being five $\sqrt{2}$ size intervals smaller than the crushing limit (i.e. it was one-eighth of the crushing limit) with a maximum value of 3353μm.

Within the abrasion-to-crushing transition zone, a simple linear transition of the type

$$B=a\,B_1+(1-a)B_2$$

was used,

where B_1 is the abrasion breakage function,

B_2 is the crushing breakage function, and

a is the proportion of the distance (in size-interval terms) across the transition zone.

The Breakage Function Matrix

The abrasion, crushing, and transition breakage matrices were finally combined into a single three-part matrix, the general scheme of which is shown in Fig. 3. Computation of the breakage-rate functions and discharge-rate functions could then be carried out.

Characteristics of the Experimental Breakage-rate Functions

Fig. 4 shows typical breakage-rate (R) and discharge-rate (D) functions computed from the test results. Starting from medium values in the coarsest sizes, the breakage-rate function rises rapidly to a peak at the crushing limit; as crushing breakage begins to appear, the breakage rate plunges to very low values for several size intervals (these are the 'critical sizes' in the autogenous mill) but commences to rise towards another peak as the abrasion-to-crushing zone is traversed. This second peak is usually the first of several pseudo-peaks occurring at the crest of the main crushing breakage-rate peak. After the last of these pseudo-peaks has been passed, the breakage rate declines rapidly as the finest sizes are approached, although it usually shows a final upward kick in the finest interval defined, namely the minus 76 plus 53μm fraction (the model assumes that no breakage occurs in the minus 53μm fraction).

The infinitely large breakage rate for the largest size in the example given is typical, and is due to the absence of material of that size in the load at the end of the test, in spite of the fact that it formed part of the feed. The rate of feeding of this coarsest material was, however, so low (about one piece in three hours) that none was present in the load at the conclusion of the test.

The discharge rates, D, are by definition zero for all sizes from the coarsest down to the mill discharge-grate size (4760μm). The test values then rise relatively steeply over several size intervals, after which they tend towards a constant plateau value. The discharge rate of the mill water approximates also to this plateau value.

The Essential Problems of Autogenous Mill Modelling

The basic perfect-mixing model shows that if A, R, S, and the mill feed are given, the mill contents and product can be calculated. Modelling of the autogenous mill is therefore essentially the modelling of the three parameters.

The basis of the A matrices used in this work has already been given; this leaves the modelling of the breakage and discharge function still to be described.

MODELLING OF BREAKAGE-RATE FUNCTIONS

Rates of Pebble Wear

The approach to modelling of breakage rates in the abrasion-breakage zone was through a study of pebble-wear rates or weight loss rates, as defined by

$$\text{Wear rate (weight/time)}=\frac{\text{(average weight of pebble entering size interval}-\text{average weight of pebble leaving size interval)}}{\text{Average residence time in size interval}} \quad \ldots\ldots\ldots\ldots\ldots (5)$$

Wear rates were then converted to breakage rates R for use in the model.

The general formula for residence time is

$$\text{Residence time}=\frac{\text{Quantity contained}}{\text{Entry rate}}$$

The 'quantity contained' was the weight in each $\sqrt{2}$ size interval of the mill load.

The 'entry rate' to any size interval has two components: the new feed to that interval, and the material entering the interval from coarser sizes within the mill. The fact that the new feed has a distribution across the size interval, and that its residence time in the interval is therefore distributed, was accounted for by the usual method of assuming that all the feed had the maximum size of the interval but that its rate was only half the actual feed rate to the interval.

To arrive at the entry rate to a size interval of material from coarser intervals, use was made of a 'conservation of numbers' hypothesis based on the nature of abrasion breakage, i.e. size reduction by the detachment of fine material from the surface of a central 'core'. In steady-state abrasion, therefore, the number of cores per unit time entering a size interval from coarser intervals is simply the sum of the numbers of pieces fed per unit time to all those coarser intervals. The weight flowrate into the receiving interval is the number of pieces entering per unit time multiplied by the average weight per piece at the top size of the interval.

Thus the residence time in a size interval is obtained from

$$\text{Residence time in } n\text{th interval}=\frac{\text{Weight in } n\text{th interval}}{(\frac{1}{2}\text{ weight/unit time fed to } n\text{th interval})+E}, \quad (7)$$

where E=weight flowrate from all coarser intervals.

$$E=\left(\sum_{1}^{n-1}\frac{\text{Weight/time added to interval}}{\text{Average weight/piece in interval}}\right)\times \text{Weight/piece entering } n\text{th interval}. \quad (8)$$

The average weight per piece in an interval, W_m, was defined by

$$w_m=k(d_m)^3, \quad (9)$$

where d_m is the geometric mean between top and bottom sizes (d_t and $d_t/\sqrt{2}$) of the interval, and k is a constant including density and shape factor.

Equations (6) and (7), however, give the average residence time, not of the cores alone, but of the cores *plus* the material abraded from them. The residence time of the cores alone is given by

$$\text{Residence time of cores}=\frac{\text{Weight in interval}}{\text{Mean weight flowrate of cores through interval}} \quad (10)$$

$$\text{Mean weight flowrate of cores}=\text{Effective number of pieces entering per unit time} \times \text{mean weight/piece in interval.}$$

Now,

$$\text{Mean weight/piece in interval}=\text{Weight/piece at top of interval}\times\frac{\text{Mean weight/piece in interval}}{\text{Weight/piece at top of interval}}.$$

Therefore, from equation (9),

$$\text{Mean weight/piece in interval}=\text{Weight/piece at top of interval}\times\frac{k(d_t(d_t/\sqrt{2}))^{3/2}}{k(d_t)^3}$$

$$=\text{Weight/piece at top of fraction}\times 2^{-\frac{3}{2}}$$

$$=\text{Weight/piece at top of fraction}\times\frac{1}{1,706}.$$

Therefore, equation (7) is modified to

$$\text{Pebble residence time in } n\text{th interval}=\frac{\text{Weight in } n\text{th interval}\times 1,706}{(\frac{1}{2}\text{ weight/time added to } n\text{th interval})+E}. \quad (11)$$

Pebble wear rate is then given by equation (5).

Table V shows the method for the calculation of wear rate and the results for a typical Cobar test, while, in Fig. 5, log pebble-wear rate is plotted against log pebble size for three of the tests. The plotted points can in each case be reasonably well fitted by two straight lines of slope 3 and 2 respectively, intersecting at 53648μm. The slope of 3 implies pebble wear proportional to the cube of pebble size (i.e. proportional to pebble weight), while a slope of 2 implies wear proportional to pebble surface area.

Similar results were obtained in all Cobar tests, so that it can be said that, under the conditions obtaining in these tests, Davis-type wear[8] occurs in pebbles down to 53648μm in size and Prentice-type wear[9] from that size down to the crushing limit.

Factors Controlling Pebble-wear Rates

If the wear rate at the changeover size from weight-dependent to surface-dependent wear can be predicted, the wear rates at all other sizes down to the abrasion limit follow very simply, since, for weight-dependent wear, log wear rates for the successive $\sqrt{2}$ size intervals form an arithmetic progression with common difference 0,4512 (i.e. $3\times\log\sqrt{2}$), while for surface-dependent wear the progression is also arithmetic with common difference 0,3008 (i.e. $2\times\log\sqrt{2}$). Regression analysis of the factors that might control the wear rate at the changeover size yielded the following relationship

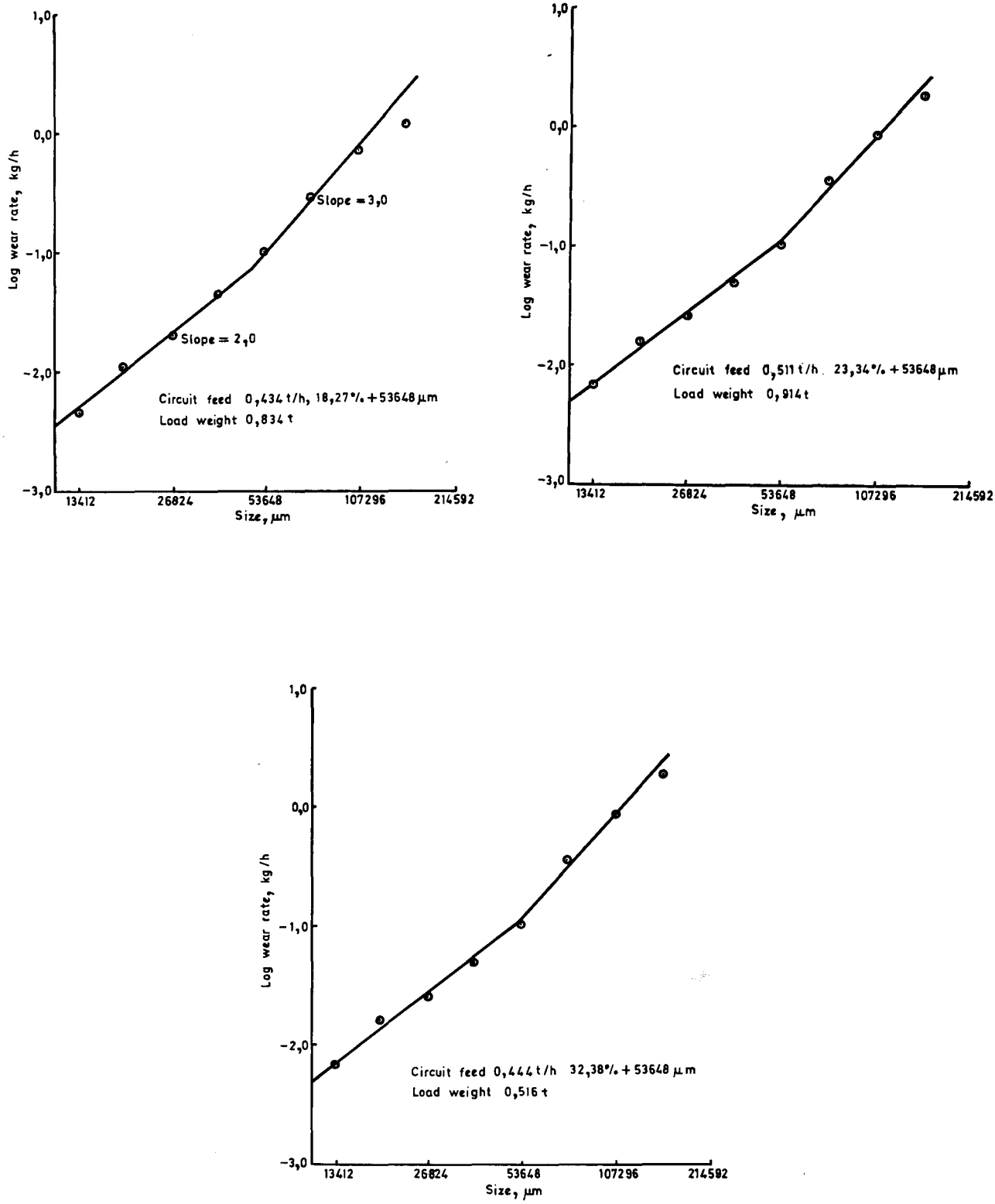

Fig. 5—Rate of pebble wear *versus* pebble size

$$\text{Wear rate at } 53648\mu\text{m (kg/h)} = 0{,}0071 \times (\text{circuit feed cumulative } \% + 53648\mu\text{m}) \times \left(\frac{500}{\text{Weight of dry load (kg)}}\right)^{0{,}71} \quad \ldots\ldots\ldots\ldots (12)$$

The quantity 500 is simply a standard dry load weight to which the wear rates are corrected. Mill discharge density was insignificant in the range 60 to 80 per cent.

Equation (12) provides a significant insight into the functioning of the grinding media in the autogenous mill (and indeed in all tumbling mills) because it shows, not only that the wear rate is dependent on the sizing of the media, but that it is also inversely related to the quantity of the mill load (i.e., as the weight of the load *decreases*, the wear rate of the grinding media *increases*). This is a phenomenon well known to pebble-mill operators, and can be explained as follows. The mill load is imagined to be an epicyclic gear running on the inner surface of the mill; the smaller the mill load, the faster it will rotate and the higher will be the rate of pebble wear.

Because pebble-wear rates are partly dependent on total weight of mill load, the pebble portion of the load cannot be predicted alone. Furthermore, since weight of load is in turn dependent on pebble-wear rates, an iterative method of computation of the entire mill load has to be adopted in which convergence is obtained between a function relating pebble wear direct to load weight and the mill model, the latter being in fact a second, indirect relationship between pebble-wear rates and load weights.

The Conversion of Wear Rates to Breakage Rates

Since the mill model adopted was of the matrix type, it was necessary to convert the wear-rate model to matrix form, and the connection between the two types of model was arrived at by the following reasoning:

For equilibrium,

Weight/time entering size interval = Weight/time leaving interval.

If there is no discharge of the size fraction from the segment,

Weight/time entering = Number of pieces in interval $\times q$, ... (13)

where q = the total loss in weight from the interval per piece per unit time

= the rate at which material is abraded from the piece plus the rate at which the piece removes weight from the interval by passing into the next lower interval.

In the matrix model, the loss in weight per unit time from an interval is given by

Weight/time leaving = $(1-\alpha_1) \times$ breakage rate $(R) \times$ weight in interval, ... (14)

where α_1 = the first element in the breakage function applicable to the size interval concerned, i.e. the proportion that remains in the parent size interval after breakage.

Therefore, from equations (13) and (14),

Number of pieces in interval $\times q = (1-\alpha_1) \times R \times$ weight in interval. . . . . (15)

Since each entering piece disappears from the interval at the end of its residence time, the factor q in equation (13) is simply

$$\frac{\text{Weight of pebble at top size of interval}}{\text{Residence time}}.$$

Therefore, from equation (15),

$$\frac{\text{No. of pieces in interval} \times \text{pebble weight at top}}{\text{Residence time}} = (1-\alpha_1) \times R \times \text{weight in interval},$$

i.e.,

$$\frac{\text{Weight in interval} \times \text{pebble weight at top}}{\text{Average weight/piece in interval} \times \text{residence time}} = (1-\alpha_1) \times R \times \text{weight in interval},$$

i.e.,

$$\frac{\text{Pebble weight at top}}{\text{Average weight/piece} \times \text{residence time}} = (1-\alpha_1) \times R,$$

i.e., for a $\sqrt{2}$ size series,

$$\frac{1{,}706}{\text{Residence time}} = (1-\alpha_1) \times R. \quad \ldots\ldots (16)$$

Equation (16) relates the residence time, the essential parameter of the wear-rate model, and a and R, the parameters of the matrix model (D being zero in the pebble sizes).

Prediction of Abrasion Breakage Rates

It can be shown that, for Davis-type (i.e. weight-dependent) pebble wear, the residence times in successive size intervals in constant ratio to each other are equal. For Prentice-type (i.e. surface-dependent) wear, the residence times in successively increasing size intervals in constant ratio to each other are in the same ratio as the intervals.

Therefore, from equation (16), it follows that the breakage-rate function will be constant for those size intervals in which Davis-type wear occurs, and will then increase exponentially with decreasing size in the Prentice wear zone until the crushing limit is reached. Thus, if the pebble-wear rate in any one size interval can be predicted and the changeover point between the two types of wear is known, the breakage rates for all sizes above the crushing limit follow automatically.

Equations (4), (5), (12), and (16) can be combined to give the breakage rate for the Cobar tests in the 53468μm size interval, the changeover size from Davis- to Prentice-type wear—see equation (17).

$$R_{(53648)} = \frac{0{,}0213 \times (\text{circuit feed } \% + 53648\mu\text{m}) \times \left(\frac{500}{\text{Load weight}}\right)^{0{,}71}}{(1-\alpha_1)} \quad \ldots (17)$$

TABLE V

CALCULATION OF PEBBLE-WEAR RATE

(1) Size	(2) Feed rate	(3) ½ feed rate	(4) Average weight at top of size fraction	(5) Average weight at mean of size fraction	(6) Number of pieces fed to mill per hour	(7) Cum. no. of pieces per hour from larger sizes	(8) Cum. weight per hour from larger sizes	(9) Effective weight entering per hour	(10) Weight in load	(12) Residence time of pebbles	(13) Average wear rate
μm	kg/h	kg/h (2)/2	kg	kg	(2)/(5)	Σ (6)	kg/h (4)×(7)	kg/h (3)+(8)	kg	h (10)×1,706/(9)	kg/h
214 592	0,24	0,12	56,27	33,47	0,007	Nil	Nil	0,12	Nil	—	—
151 712	13,77	6,89	19,91	11,83	1,16	0,01	0,19	7,08	44,97	10,84	1,19
107 296	10,09	5,05	7,04	4,19	2,41	1,17	8,24	13,29	49,90	6,41	0,71
75 856	18,29	9,14	2,49	1,48	12,37	3,58	8,91	18,05	60,01	5,67	0,28
53 648	36,81	18,40	0,88	0,523	70,57	15,95	14,04	32,44	107,99	5,68	0,10
37 928	47,49	23,75	0,31	0,185	255,41	86,52	26,82	50,57	134,32	4,51	0,045
26 824	46,54	23,27	0,11	0,063	733,07	341,93	37,61	60,88	118,10	3,33	0,021
18 964	39,30	19,65	0,039	0,023	1699,22	1075,00	41,93	61,58	84,83	2,35	0,011
13 412	33,95	16,98	0,014	0,008	4159,44	2774,22	38,84	55,82	59,34	1,85	0,0048

Davis-type abrasion	Prentice-type abrasion	Transition zone			Crushing breakage
a 0 0 . .	0 0 0 0 .	0	0	0	. . 0 0 0 0
b a 0 . .	0 0 0 0 .	0	0	0	. . 0 0 0 0
c b a . .	0 0 0 0 .	0	0	0	. . 0 0 0 0
d c b . .	0 0 0 0 .	0	0	0	. . 0 0 0 0
e d c . .	0 0 0 0 .	0	0	0	. . 0 0 0 0
f e d . .	a 0 0 0 .	0	0	0	. . 0 0 0 0
g f e . .	b a 0 0 .	0	0	0	. . 0 0 0 0
k g f . .	c b a 0 .	0	0	0	. . 0 0 0 0
. h g . .	d c b a .	0	0	0	. . 0 0 0 0
. . h . .	e d c b .	0	0	0	. . 0 0 0 0
. . . . .	f e d c .	α_1a+(1−α_1)p	0	0	. . 0 0 0 0
. . . . .	g f e d .	α_1b+(1−α_1)q	α_2a+(1−α_2)p	0	. . 0 0 0 0
. . . . .	h g f e .	α_1c+(1−α_1)r	α_2b+(1−α_2)q	α_3a+(1−α_3)p	. . 0 0 0 0
. . . . .	. h g f .	α_1d+(1−α_1)s	α_2c+(1−α_2)r	α_3b+(1−α_3)q	. . 0 0 0 0
. . . . .	. . h g .	α_1e+(1−α_1)t	α_2d+(1−α_2)s	α_3c+(1−α_3)r	. . 0 0 0 0
. . . . .	w w w w .	α_1w+(1−α_1)u	α_2w+(1−α_2)t	α_3w+(1−α_3)s	. . p 0 0 0
. . . . .	x x x x .	α_1x+(1−α_1)v	α_2x+(1−α_2)u	α_3x+(1−α_3)t	. . q p 0 0
. . . . .	y y y y .	.	α_2y+(1−α_2)v	α_3y+(1−α_3)u	. . r q p 0
. . . . .	z z z z .	.	.	α_3z+(1−α_3)v	. . s r q p

Fig. 6—The four-part matrix used for the Cobar model

The R factors for all sizes coarser than 53648μm are then the same as that at 53648μm, while, for smaller sizes down to the crushing limit, the factors are calculated from the relationship $R_n=\sqrt{2}.R_{n-1}$ (n=number of size interval, increasing with decreasing size).

Modification of the Appearance Matrix

Because the studies of pebble-wear rate showed that two types of abrasion breakage occurred in the Cobar tests, the three-part breakage-function matrix shown in Fig. 3 had to be modified accordingly. This necessitated the devising of breakage functions to describe weight-dependent and surface-dependent abrasion respectively.

Weight-dependent abrasion is postulated as being chipping breakage, i.e. breakage resulting from the breaking-off of edges and corners or from a crack network confined to a relatively thin surface layer of the parent particle. It was therefore felt that the original abrasion function shown in Table II adequately described this type of breakage.

As regards surface-dependent abrasion, it seemed reasonable to postulate that the size distribution of the fragments that are supposedly torn from the pebble surface by friction would remain constant regardless of the size of the pebble. Hence, the breakage function would again show the bulk of the parent pieces remaining in the original size interval and a mathematically related proportion appearing in the next smaller fraction, but the detritus would appear in the same, considerably smaller, size intervals regardless of the size of the original pieces. Thus, the basic function describing surface-dependent abrasion was the same as for weight-dependent abrasion, but the computing programme included provision for the retention of the lower terms of the function in the same size intervals, regardless of the intervals in which the top terms appeared.

The appearance matrix eventually used for the Cobar model was thus a four-part one, containing two sections in the abrasion portion built up from the functions just proposed, a changeover section, and finally a

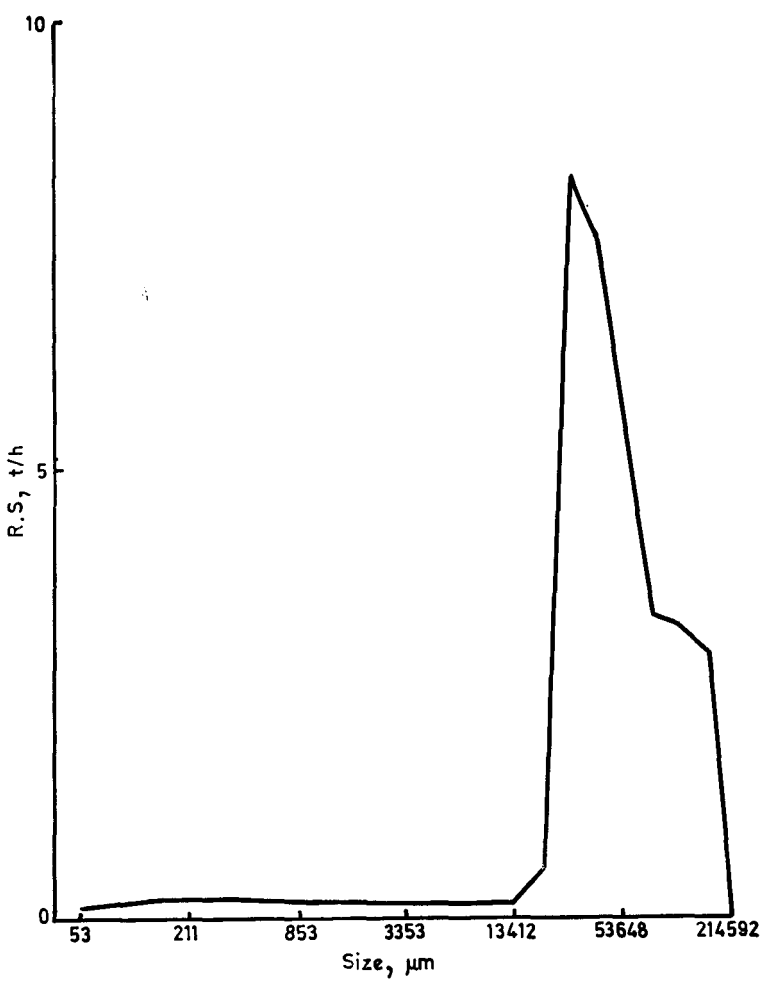

Fig. 7—Weight broken per unit time *versus* size

pure crushing section. This is indicated in Fig. 6.

Crushing Breakage Rates and their Prediction

As indicated by the dotted lines in Fig. 4, the crushing breakage portion of the rate curve can be reasonably closely simulated by two intersecting straight lines of slope +1,0 and −1,0 respectively. This was true for all the Cobar tests, and, since breakage rates are also measures of the probability of breakage, the implication is that the probability of crushing breakage increases inversely with decreasing size to a maximum and thereafter decreases directly with decreasing size. This implication seemed of considerable significance, and confirmation was sought in the literature.

Unfortunately, no information on the breakage rate for autogenous mills could be found, although a number of authors have published such data for ball mills[2,6,10], and Lees[2] has computed breakage rates from rod-mill data published by Myers and Lewis[11]. These data, as is to be expected in correctly operated non-autogenous mills, show only the positive slope of the crushing-breakage peak. The slope is usually about 1,4, i.e. somewhat steeper than in the Cobar mill. The only other breakage-rate data for an autogenous mill known to the author are those obtained in a test conducted by him on a 5,1m diameter by 5,2m long mill grinding a quartz-magnetite copper ore in the Warrego concentrator, Northern Territory, Australia. The slopes in that case were +1,38 and −1,38 (Fig. 18).

The Relationship between Crushing Breakage Rate and Load Size Distribution

The breakage rate, R, is the quotient of the weight broken per unit time in a size interval by the weight of the load in that interval:

$$R=\frac{R.s}{s}.$$

Therefore, the more nearly constant is the weight broken per unit time ($R.s$) over a range of size intervals, the more nearly will the size distribution of the load over the same size range approximate the reciprocal of the breakage-rate function. In the Cobar tests, the $R.s$ values had a noticeable tendency to constancy over the size range covered by the crushing breakage peak (Fig. 7), and the load size distributions therefore all showed a valley with side slopes of +1 and −1 corresponding to the breakage rate peak (Fig. 8).

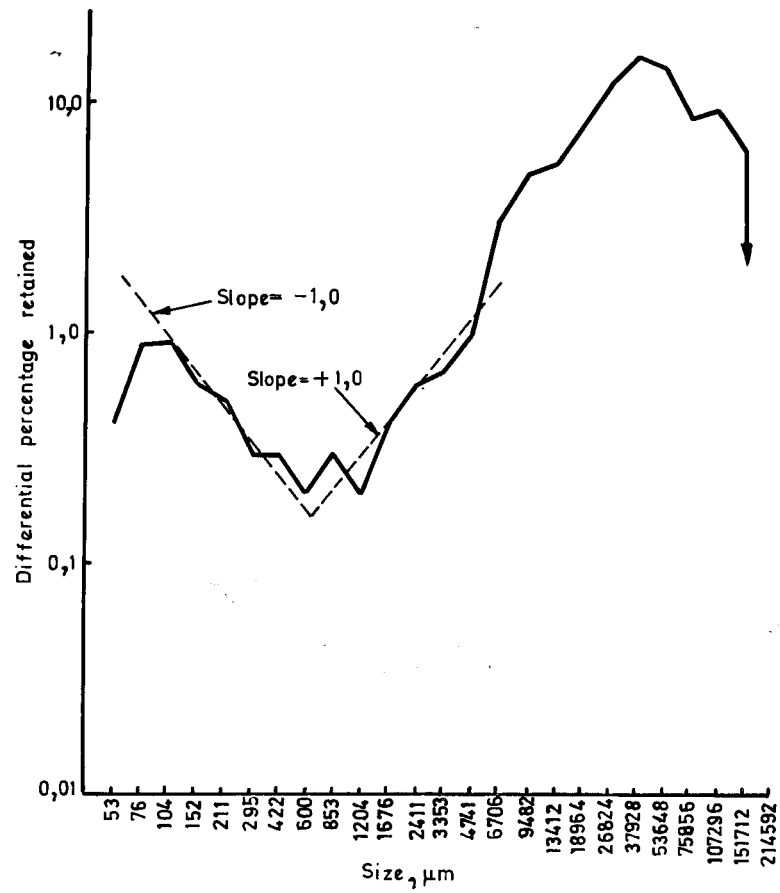

Fig. 8—Size distribution of the load, Cobar pilot mill

The size distribution of the load in the Warrego mill test also showed a +1 and −1 valley (Fig. 9), although the breakage-rate peak had side slopes of +1,38 and −1,38. This is due to the marked curvature in the graph of $R.s$ *versus* size computed for this test, which may have been the result of inaccuracy in the feed sizing since the feed size distribution was known with much less accuracy than in the Cobar tests.

To obtain some further confirmation of the general form of the crushing breakage-rate peak, the only other known autogenous and semi-autogenous load size distributions were also transposed onto $\sqrt{2}$ size intervals and plotted on log-log axes. These load sizings were published by Jackson[12] and are for 4,2m diameter by 4,9m long mills grinding Witwatersrand gold ore fully autogenously and semi-autogenously respectively. Again, the fully autogenous mill shows a +1 and −1 valley in its load size distribution (Fig. 10), while the semi-autogenous mill has slopes of +1,4 and −1,4 (Fig. 11).

From these observations, the following conclusions were drawn.

(1) A valley of side slopes +1 and −1 in the crushing breakage zone is characteristic of the log-log differential load size distribution in an autogenous mill. For ferrous-medium mills, only the negative slope is normally evident, and its value is usually about −1,4.

(2) In autogenous mills, the log-log crushing breakage-rate function is characteristically a symmetrical straight-sided peak, the slopes of which differ among mills. The factors controlling the slopes are as yet unknown. For ferrous-medium mills, only the positive slope is normally evident, and its value is usually

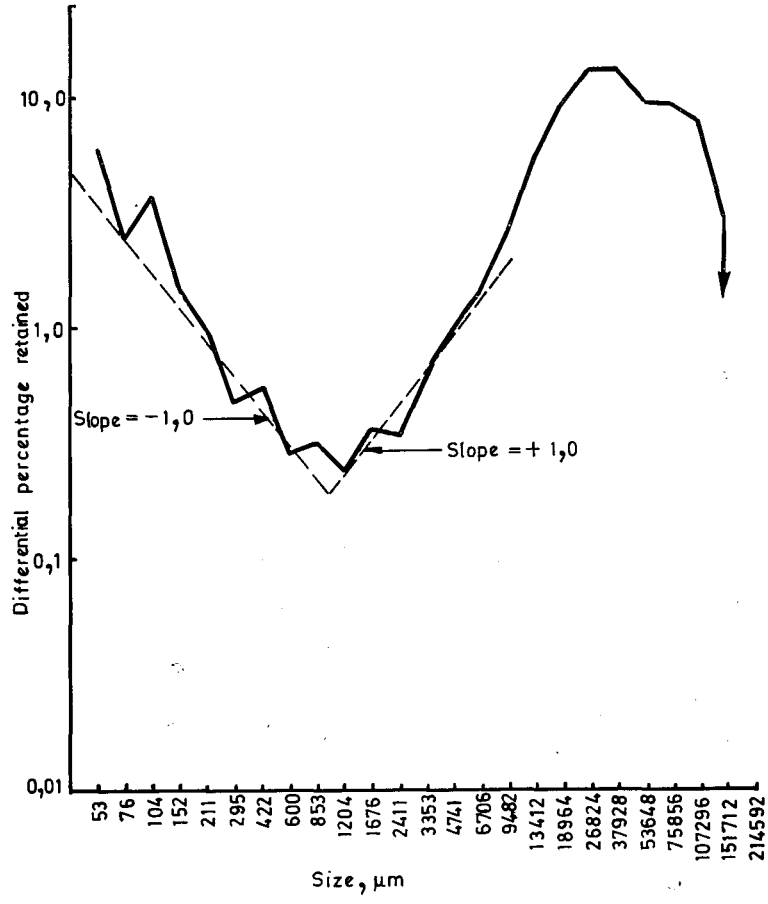

Fig. 9—Size distribution of the load, Warrego.

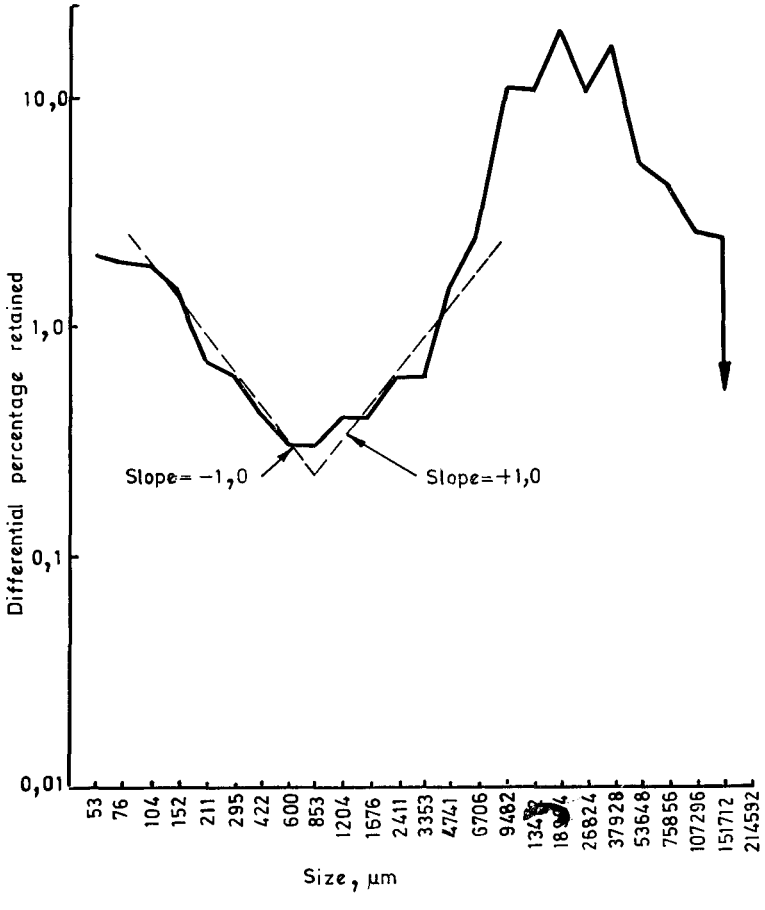

Fig. 10—Size distribution of the load, Leslie

about 1,4.

The Prediction of Autogenous Crushing Breakage Rates

From the second of the above conclusions, it follows that the problem of simulating the crushing breakage-rate function in autogenous mills comprises three elements:

(a) fixing the size at which the peak breakage rate occurs,
(b) determining the magnitude of the peak, and
(c) determining the side slopes of the peak on log-log axes.

As regards the first of these elements, it was found that the size at which the peak crushing breakage rate occurs in the Cobar tests was related to the circuit feed sizing by the equation

Log_{10} size (μm) at breakage peak = 2,63 + (0,014 × circuit feed % + 107296μm). . . . . (18)

The magnitude of the breakage-rate peak was found to be controlled by three factors:

(i) the net mill energy input per unit weight of ore fed to the mill (new feed plus circulating load)*,
(ii) the weight of dry load (presumably as a measure of the 'epicyclic gear' effect suggested in the discussion of pebble wear), and
(iii) the concentration in the pebble portion of the circuit feed of a 'most effective' pebble size.

The relationship eventually determined was

$$\text{Peak crushing breakage rate} = 35,3 \times \text{kWh/tonne of total feed} \times \left(\frac{500}{\text{Load weight (kg)}}\right) \times \left(\frac{\text{Circuit feed \%} - 151712 + 53648\mu\text{m}}{\text{Circuit feed total \%} + 53648\mu\text{m}}\right) \quad . . \quad (19)$$

Finally, the side slopes of the breakage-rate peak were taken to be +1,0 and −1,0, and simulation of the crushing breakage portion of the rate curve was then possible. This was combined with the predicted abrasion breakage rates to give a prediction of the entire breakage-rate function.

DISCHARGE RATES AND THEIR PREDICTION

The problem of simulating the discharge function of the Cobar mill (and that of any non-overflow mill) can be reduced to two elements:

(1) determining the magnitude of the plateau value of the function (D_{max}), and
(2) determining the maximum size to which the plateau extends (size D_{max}).

The end of the plateau is then connected to the series of zero values commencing at the discharge aperture size by means of an S-curve of the form

$$D(I) = D_{max} \frac{(x-b)^2\ (2x-3a+b)}{(b-a)^3},$$

where x = log size at $D(I)$,
a = log size D_{max}, and
b = log aperture size of mill discharge.

Analysis of test results showed that D_{max} was controlled by two factors:

(a) the pulp density of the mill discharge (decreasing linearly with increasing density), and
(b) the size distribution of the load, while size D_{max} depended only on the pulp density of the discharge, increasing with this quantity.

The prediction equations for the D functions were as follows:

$$D_{max} + 0,897\ (\text{discharge \% solids} - 70) = 130\ \left(\frac{\text{Weight of load} + 37929\mu\text{m}}{\text{Weight of load} + 4741\mu\text{m}}\right) - 56,9 \quad . . . . . (20)$$

and

$$\text{Log}_{10}\ \text{size}\ D_{max} = (0,044 \times \text{discharge \% solids}) - 0,294. \quad . . . . . (21)$$

Comments on the Prediction Equations for the D Function

The dependence of the maximum discharge rate on pulp density and size distribution in the load indicates that, in low-discharge grate mills at any rate, pulp has to find its way *through* the mass of grinding media to reach the discharge grate, and is not discharged from some sort of classifier pool extending along the 'toe' of the cascading load. This implies that the bulk of the pulp is located in the interstices of the load. The significance of the quantity $\frac{\text{Weight of load} + 37929\mu\text{m}}{\text{Weight of load} + 4741\mu\text{m}}$ is that it is in effect a distribution modulus and, as such, is an index of the permeability of the load by the pulp, i.e. of the ease with which the pulp can flow through the load. Likewise, the pulp density (or more likely, the related property, viscosity) also controls the ease of flow through the media to the discharge grate. The direct dependence on pulp density of the maximum size to which the maximum discharge rate extends is simply the result of increasingly dense pulps being able to keep increasingly large particles in suspension and moving towards the discharge grate. Thus, an increase in pulp density will have the effect of increasing the residence times of some particle sizes but diminishing those of others.

FURTHER RELATIONSHIPS REQUIRED

The relationships between feed characteristics and the essential parameters of the perfect mixing model of the Cobar pilot mill have now been described. However, two further relationships are required before predictions can be made with the model.

Since the prediction method for breakage rates involves the mill energy per unit mass of mill feed, and mill power depends on the weight of the load, it is first necessary to obtain a relationship between the latter two quantities. Also, since an iterative technique for the calculation of the mill load is employed, a relationship between weight of load and rate of pebble wear, other than the model itself, is required with which the model can converge.

The Relation between Load Weight and Mill Power

Net mill power for each test (i.e. indicated power from kilowatt-hour meter less empty mill power) was plotted against the log weight of dry load (Fig. 12), giving the relationship

Net mill power (kW) = 12,1

*Subsequent to the completion of the present work, Herbst and Fuerstenau[13] published the same relationship for a laboratory dry batch ball mill.

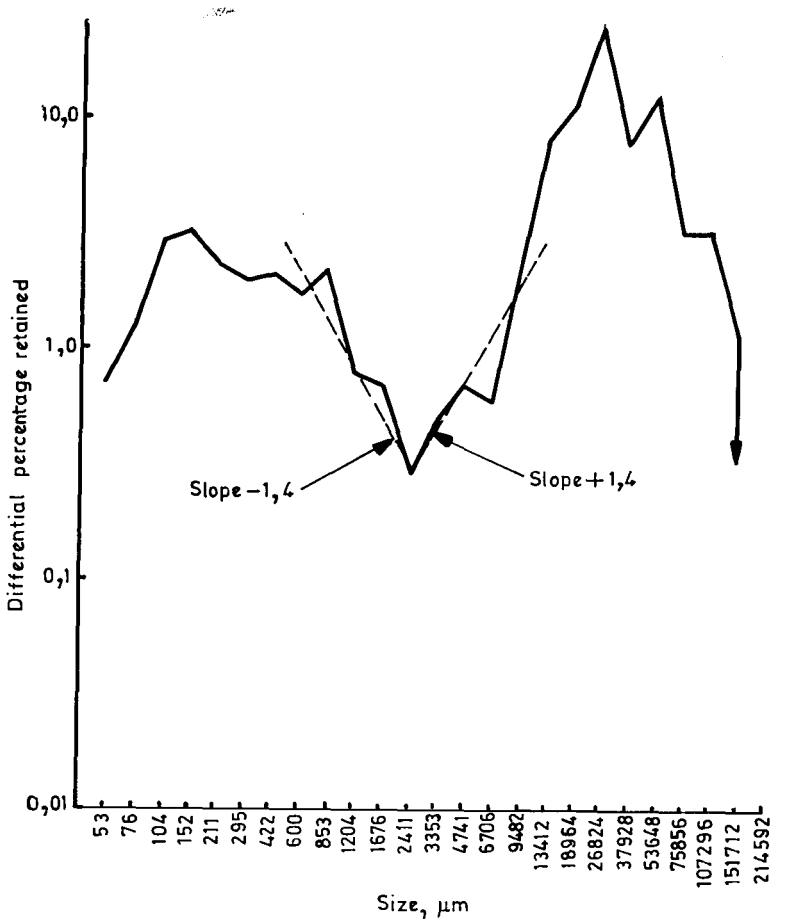

Fig. 11—Size distribution of the load in the semi-autogenous Bracken mill

($\log_{10}$ weight of dry load (kg)) − 26,4. . . . . (22)

This relationship obviously cannot be extrapolated much beyond the test conditions, since it implies both zero net power with an appreciable mill load (152kg) and also indefinite increase of power with load. Nevertheless, it was incorporated in the mill model with a 1000kg limit on computed weight of load.

The Relation between Pebble-wear Rate and Load Weight

To obtain an independent relationship between pebble-wear rate, feed sizing, and load weight with which the model could converge, it was postulated that the pebble-wear rate in the minus 75856μm plus 53648μm fraction was related to load weight by an equation of the form

$$\text{Pebble-wear rate} = \frac{C.\ (\text{circuit feed } \% + 53648\mu\text{m})}{(\text{Load weight})^x}$$

and to determine the constant C for various arbitrary values of x, finally selecting the values of C and x that gave the best fit to the experimental data. The resulting equation was

$$\text{Pebble-wear rate (kg/h) at } 53648\mu\text{m} = \frac{0{,}14\ (\text{circuit feed } \% + 53648\mu\text{m})}{(\text{Load weight (kg)})^{0{,}5}}. \quad . . . . . (23)$$

RESULTS OBTAINED USING THE MODEL

The original model gave predictions of load weight that were too high at low pebble-wear rates and *vice versa*. Since the predicted wear rates themselves agreed closely with those in the analysis of pebble-wear rate already described, it was apparent that the fault lay in equation (16), the conversion from residence time to abrasion breakage rate.

For the 53648μm size interval of the Cobar Eastern ore, and with $\alpha_1 = 0{,}99$, equation (16) converts to

$R = 300 \times$ wear rate, ... (24)

where wear rate is in kg/h.

To correct the prediction inaccuracies mentioned, it was necessary to add a correction to equation (24), which then became

$R = (300 \times \text{wear rate}) + 120\ (\text{wear rate} - 0{,}082)$. . . . . (25)

By use of equation (25), reasonably accurate predictions of load weight were obtained, as shown in Fig. 13. An example of predicted, as compared with actual, breakage-rate and discharge-rate functions is given in Fig. 14, and the predicted and actual size distributions of mill load and product are given for the same test in Fig. 15. Generally good agreement between predicted and actual size distribution is evident, in spite of obvious discrepancies in the breakage and discharge rates. In particular, the approximation of the multiple crushing peaks by a single peak does not appear to affect the predictions of size distribution significantly, and neither does the generally inaccurate prediction of D_{max}. On the other hand, the vital importance of accuracy in the prediction of abrasion breakage rates has been evident in all results, for, where the discrepancies in this parameter are greatest, the lowest overall accuracy of prediction is obtained. The model is far more sensitive to the abrasion than to the crushing breakage rates. It is unfortunate that, because of the small numbers of pebbles in the circuit feed and the resulting small numbers in the mill loads, it is also in the largest sizes that the experimental data are least accurate. Clearly, autogenous milling tests aimed at model building should be done on the largest possible scale.

MODELLING OF AN INDUSTRIAL-SCALE AUTOGENOUS MILL

Almost coincident with the completion of the steady-state model of the Cobar pilot mill, an oppor-

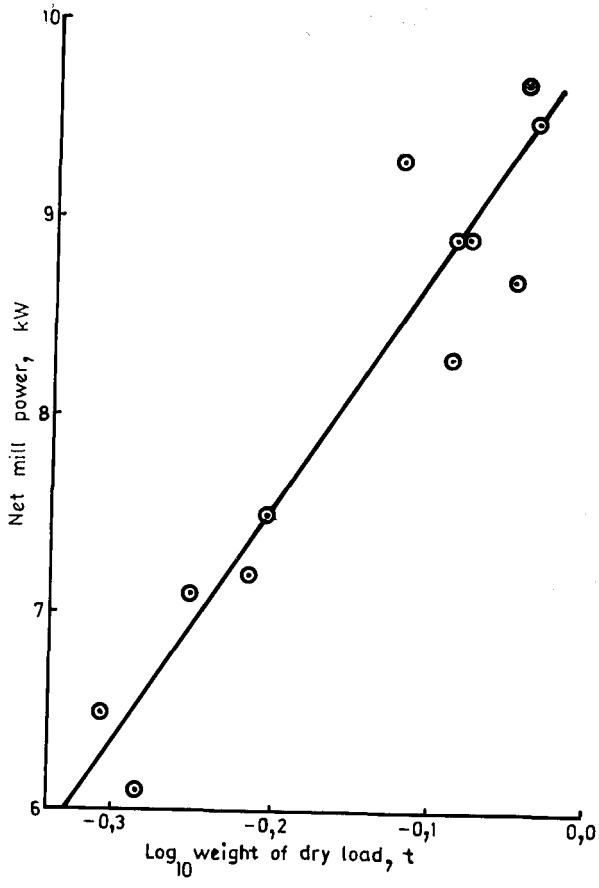

Fig. 12—Net mill power *versus* log weight of dry load

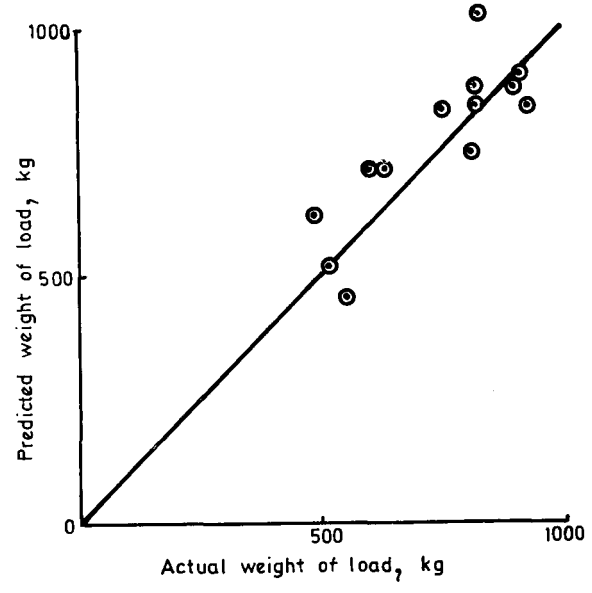

Fig. 13—Accuracy of predictions of load weight

tunity arose to confirm its general form on an industrial scale in the Warrego concentrator of Peko-Wallsend Ltd, approximately 60km west of Tennant Creek, Northern Territory, Australia.

The primary grinding circuit at Warrego comprises a single 5,1m diameter by 5,2m grate-discharge run-of-mine autogenous mill in closed circuit with a nest of five Krebs D15B 38cm cyclones. The mill is driven by a 1700kW motor at 13,9 rev/min (72,8 per cent N_c). Empty running power is 65kW. The ore is a quartz-magnetite carrying chalcopyrite, bismuthinite, and pyrite, with a specific gravity of about 4; its top size is controlled by a jaw crusher.

A series of tests was carried out in which the feed rate and the density of the cyclone overflow were systematically varied at one jaw-crusher setting (14,1cm). At each feed rate and cyclone-overflow density, the mill was allowed to reach equilibrium as indicated by constant power draft, and the circuit was then sampled for size analysis. The feed sample for each test consisted of a cut approximately 6m long and weighing about 0,5t taken from the feed belt after all other sampling in the test had been completed.

On completion of the first series of tests, the jaw-crusher setting was reduced from 14,1cm to 11,1cm and the series repeated.

At the conclusion of one of the tests in the first series, the load was dumped from the mill and sized. It weighed approximately 70t dry, i.e. less than half a 50-per-cent mill load. Its log-log differential size distribution is given in Fig. 9, and the cumulative distribution in Fig. 16.

The Empirical Model

From the test results, a simple empirical model relating crusher setting, feed rate, and cyclone-overflow density to the percentage of minus 200 mesh material in the cyclone overflow was derived. This model has been described in another paper[14], from which Fig. 17 is reproduced.

Fig. 17 shows the relation between feed rate and mill power for the Warrego mill at two crusher settings. As predicted by the Cobar model,

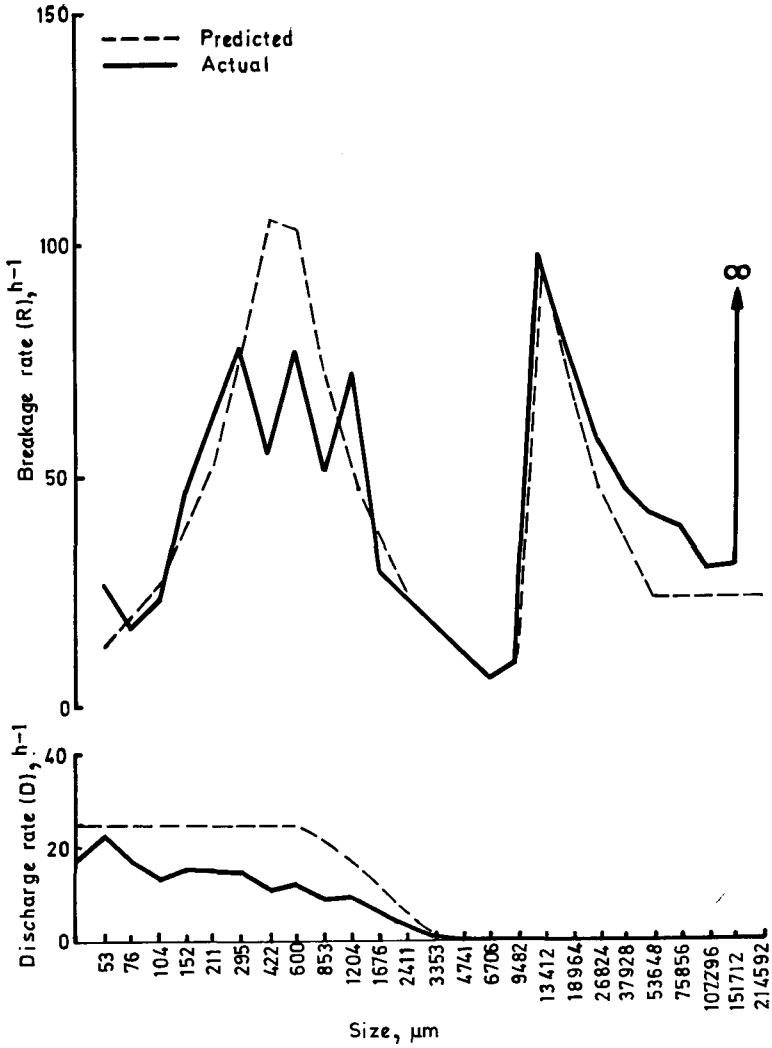

Fig. 14—Predicted and actual breakage-rate and discharge-rate functions

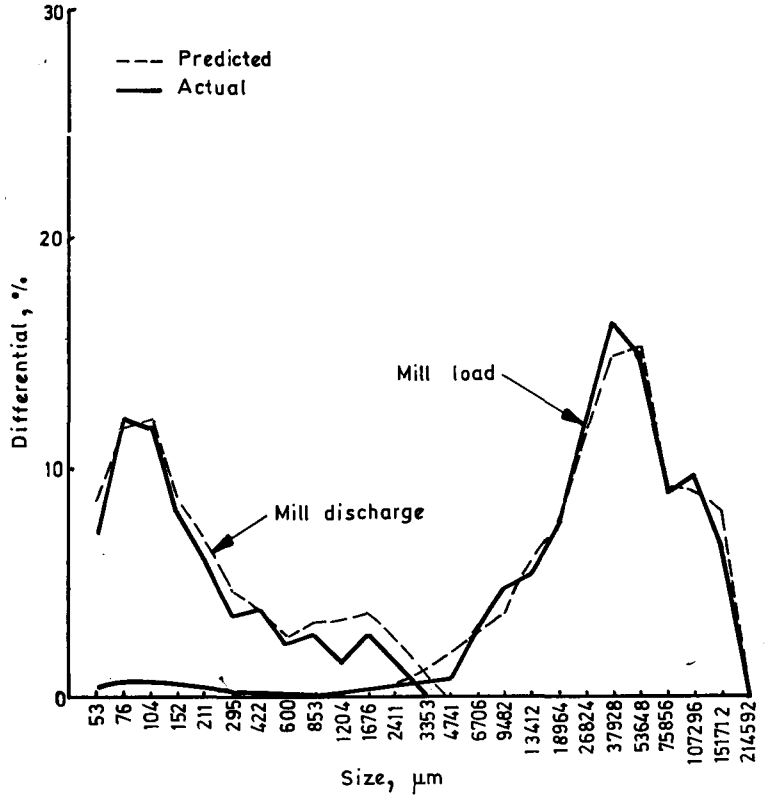

Fig. 15—Predicted and actual size distributions of mill load and product

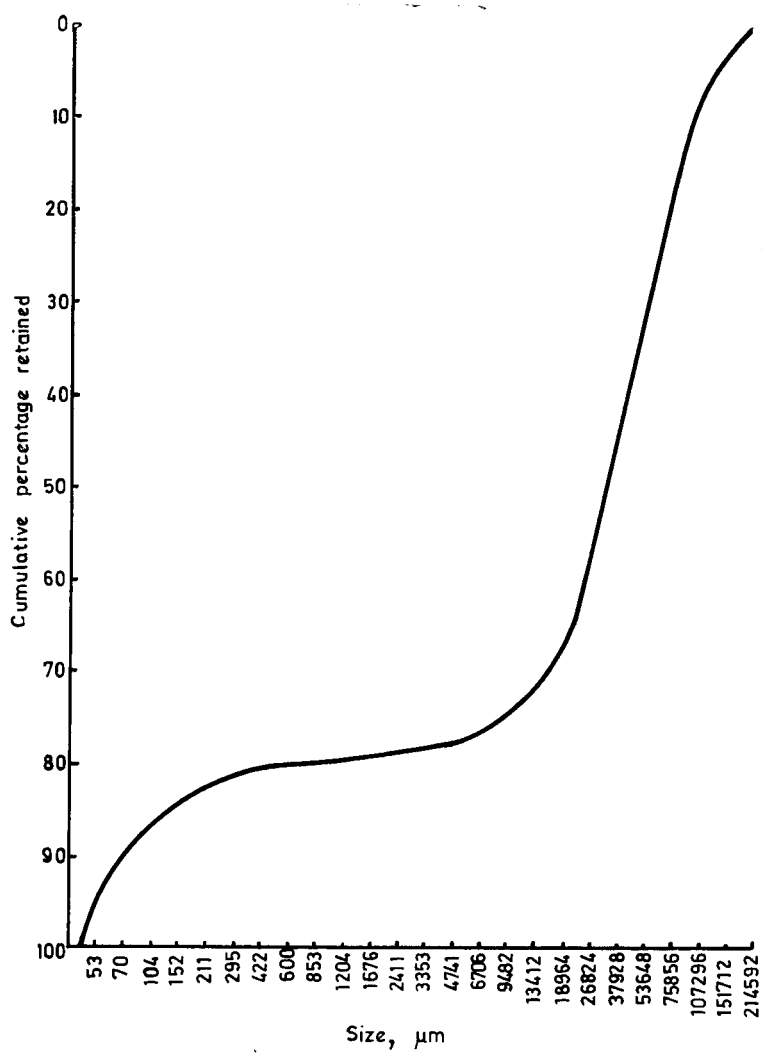

Fig. 16—Cumulative size distribution of the Warrego mill load

mill power increases with feed rate, the rate of increase depending on the crusher setting and greater settings giving smaller slopes. This follows from equation (12), which shows that increasing feed coarseness causes increasing pebble wear, resulting in a reduced load weight and hence reduced mill power. Fig. 17 shows a linear relation for feed rate *versus* mill power for both crusher settings, i.e. at the low mill-load volume percentages of the Warrego tests, the kilowatt-hours per tonne milled are independent of feed rate so that, provided classification capacity can be varied to suit circuit feed rate, the proportion of minus 200-mesh material in the cyclone overflow should also be independent of feed rate. The situation with regard to changes in feed sizing is, however, much less fortunate, as here the autogenous mill reacts in a completely undesirable fashion, finer feed *increasing* the mill power draft and hence compounding the normal increasing fineness effect of the finer feed on the sizing of the final product.

Parameters of the Perfect-mixing Model

Because of the magnitude of the undertaking and the demands of production, it was possible to make only one determination of the size distribution in the Warrego mill load, and hence of breakage and discharge rates, These rates are given in Fig. 18, which shows that the breakage rate function has the same general bimodal form as obtained in the Cobar tests, while the discharge function is similar to the Cobar ones in having a plateau in the fine sizes, which then diminishes to zero at the size of the mill-discharge aperture via a flattened S-curve. The actual magnitudes of the breakage rates are higher, and of the discharge rates lower, than in the Cobar mill, while the crushing and abrasion limits are much higher, all of which differences are to be expected in the larger mill. Furthermore, the curve for Warrego breakage rates does not exhibit the exponential peak characteristic of surface-dependent pebble wear as obtained in the Cobar tests, and this, together with studies of pebble wear, indicates that only weight-dependent pebble wear occurred in the Warrego mill, presumably because of the high crushing limit. Also, as already mentioned, the slopes of the crushing breakage peak are $+1{,}38$ and $-1{,}38$, and not $+1{,}0$ and $-1{,}0$ as in the Cobar mill.

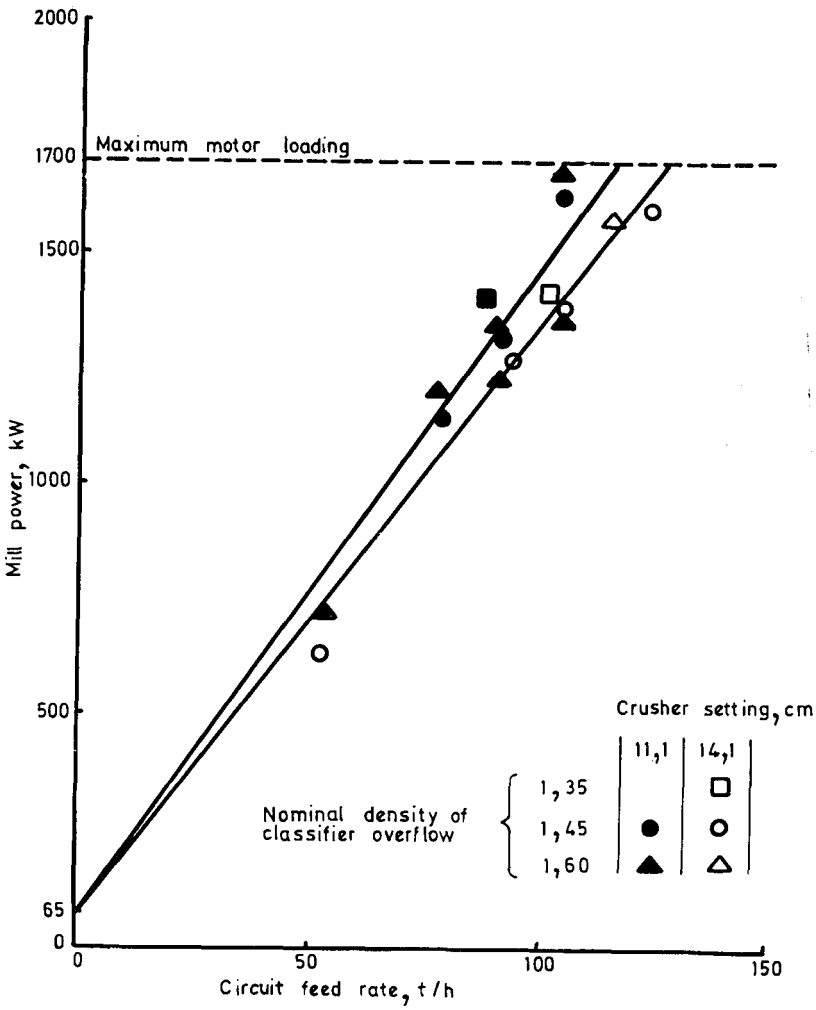

Fig. 17—Feed rate *versus* mill power, Warrego mill

Nevertheless, the general similarity of the breakage and discharge functions for the two mills indicates that the mechanisms are fundamentally the same, and that the form of the modelling equations obtained for the Cobar mill would therefore apply to the Warrego mill, only the constants being different.

The DR^{-1} Parameter

In the discussion of the theory of the perfect-mixing model, it was pointed out that, if the load size distribution s was not known, the parameters $\bar{D}$ and R could not be separated but could be obtained only as a combined parameter such as DR^{-1}. Accordingly the DR^{-1} function was computed for each of the Warrego tests, the general form of the results being as shown in Fig. 19. If DR^{-1} can be related to operating conditions, it can be used in the prediction of mill product from mill feed, although no information about the mill load can be obtained. Work on this possibility is proceeding.

CONCLUSION

It has been shown that, by inclusion of the special characteristics of the autogenous mill (in particular, the simultaneous occurrence of abrasion and crushing breakage), it is possible to develop a satisfactory steady-state model of that type of mill on the hypothesis of perfect mixing. Analysis of the factors that control the model parameters has thrown new light on the mechanism of the autogenous mill, and indeed of all types of tumbling mill. Specifically:

(1) there is a transition zone between abrasion and crushing breakage, the limits of this zone depending on feed sizing;

(2) two kinds of pebble abrasion can occur, namely weight dependent and surface dependent, and these correspond to Davis-type and Prentice-type grinding-ball wear respectively;

(3) there is an 'epicyclic gear' type of effect in the mill load that increases breakage rates as the load size decreases, presumably owing to an increase in the frequency with which particles are subjected to breakage events;

(4) crushing breakage rates are controlled by the energy input per unit mass of mill feed;

(5) crushing breakage rates are also controlled by the concentration of the optimum-sized grinding media in the feed, and the effectiveness of these optimum media is reduced by the presence of excessively large media; and

(6) discharge rates in non-overflow mills are controlled by the size distribution of the mill load and by the pulp density of the mill discharge.

However, the present work has not examined all the factors that might affect the model parameters; in particular, more research needs to be done into the effects of mill size and speed, and of ore characteristics, on pebble-wear rates. The effect of mill length:diameter ratio also awaits elucidation, and, of course, ways of overcoming the adverse reaction of the autogenous mill to increasing feed coarseness, namely that it then draws less, and not more, power, should be investigated.

Since the breakage-rate and discharge-rate functions are the essential parameters (together with the breakage function, which is presumably ore-dependent) that determine the size distribution of any mill product, knowledge of how they are controlled would offer a more rational basis for mill design than the purely empirical one now employed, and would seem to hold out the possibility of 'tailoring' pulp size distributions closer to the optimum for subsequent recovery processes than is now possible. The use of the model for mill design optimization is, however, only one of its many possible applications, and it is hoped that, now that a satisfactory model of the autogenous mill has been demonstrated, it will find widespread use in plant design and

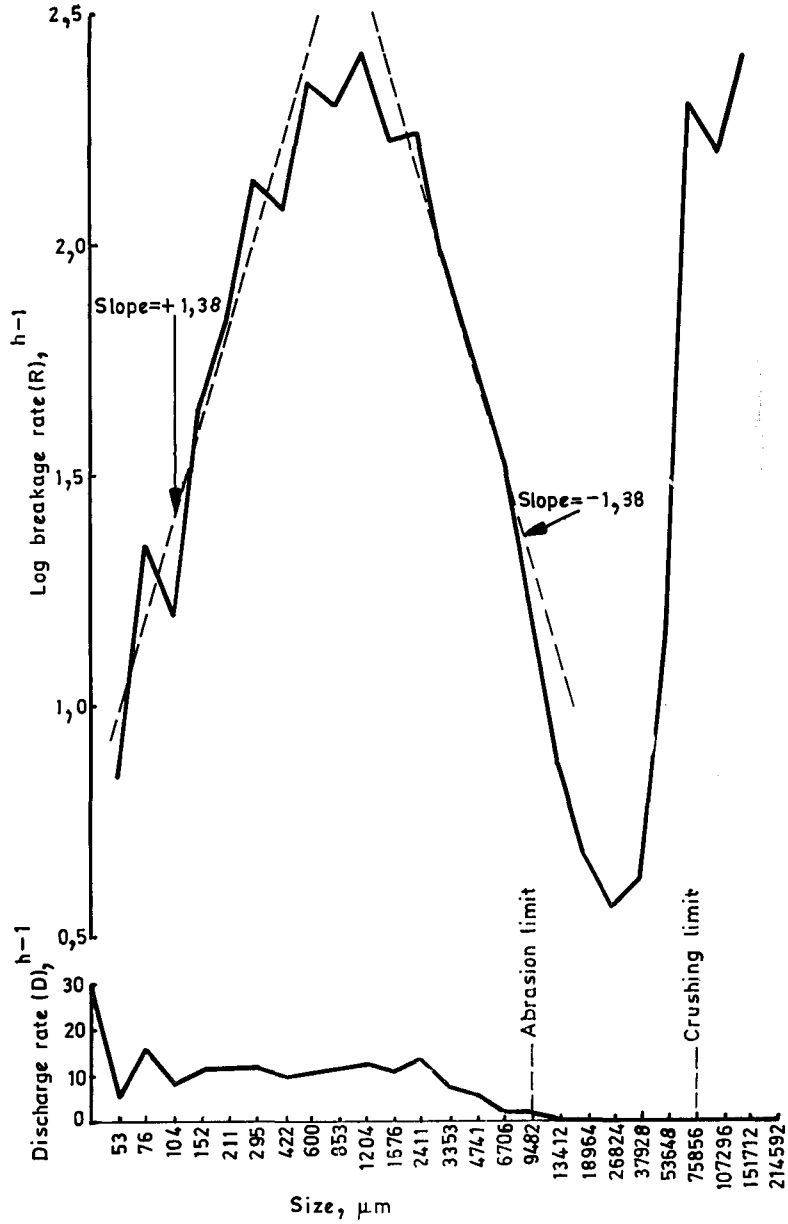

Fig. 18—Breakage- and discharge-rate functions for the Warrego mill

optimization and also in automatic control studies.

ACKNOWLEDGEMENTS

The author wishes to thank the managements of Cobar Mines Pty Ltd and of Peko Mines N.L. for the generous provision of research facilities on their properties and for permission to publish the results. He also gratefully acknowledges the award of a Research Scholarship by the University of Queensland from funds provided by Mount Isa Mines, Ltd, and of financial support and encouragement from Union Corporation Limited. Dr A. J. Lynch, Director of the Julius Kruttschnitt Mineral Research Centre, Dr W. J. Whiten, Research Officer, and many others at the Centre provided invaluable assistance that is most gratefully acknowledged. The permission of the Director General, National Institute for Metallurgy, Johannesburg, to publish this paper is also gratefully acknowledged.

REFERENCES

1. WHITEN, W. J. A matrix theory of comminution machines. *Chem. Engng Sci.*, vol. 29. 1974. pp. 589-599.
2. LEES, M. J. *Experimental and computer studies of the dynamic behaviour of an industrial grinding circuit.* Ph.D. Thesis, University of Queensland, 1973.
3. WICKHAM, P. *Comminution of pebbles and fine ores.* M.Eng.Sci. Thesis, University of Queensland, 1972.
4. BROADBENT, S. R., and CALLCOTT, T. G. Coal breakage processes. *J. Inst. Fuel*, vol. 29. 1956.
5. BUSH, P. D. *The breakage of mineral particles in ball mills.* Ph.D. Thesis, University of Queensland, 1970.
6. TAUTE, W. J., MEYER, P. H., and AUSTEN, L. G. Comparison of breakage parameters in two tumbling mills of different diameter. IFAC Symposium on Automatic Control in Mining, Mineral and Metal Processing, Sydney, 1973.
7. LYNCH, A. J., and MOORE, D. E. The mechanical breakage of mineral part-

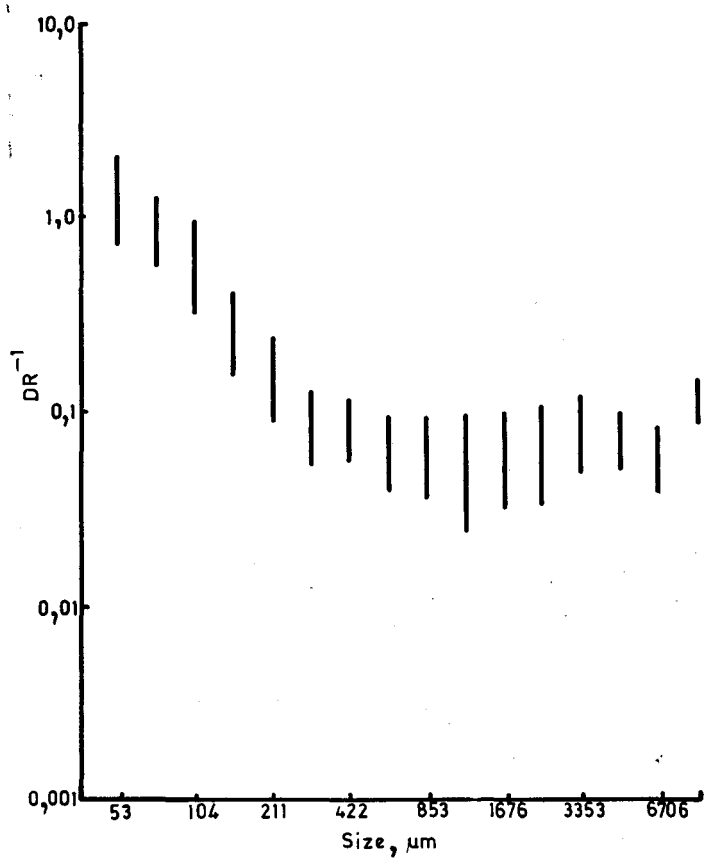

Fig. 19—The DR^{-1} function in the Warrego tests

icles. *Proceedings First Tewkesbury Symposium on Fracture*, 1963. Melbourne, Butterworth.

8. DAVIS, E. W. Fine crushing in ball mills. *Trans. AIME*, vol. 61. 1919. p. 250.
9. PRENTICE, T. K. Ball wear in cylindrical mills. *J. Chem. Metall. Min. Soc. S. Afr.*, vol. 43, nos 7 and 8. 1943.
10. REID, K. J., and STEWART, P. S. B. An analogue model of batch grinding and its application to the analysis of grinding results. *Chemica* 70, p. 87.
11. MYERS, J. F., and LEWIS, F. M. Fine crushing with a rod mill at Tennessee Copper Company. AIME Technical Publication no. 2041, *Min. Technol.*, vol. 10, no. 4.
12. JACKSON, O. A. E. Autogenous and composite load milling practice at the South African gold mines of Union Corporation Ltd. *VII International Mineral Processing Congress, New York*, 1964.
13. HERBST, J. A., and FUERSTENAU, D. W. Mathematical simulation of dry ball milling using specific power information *Trans. Soc. Min. Engrs AIME*, vol. 254. Dec. 1973. pp. 343-348.
14. STANLEY, G. G., STEVENSON, C. H., and LYNCH, A. J. Autogenous grinding in the Warrego concentrator, Peko Mines N.L. Paper delivered at the Regional Meeting, North West Queensland Branch, Australasian Institute of Mining and Metallurgy, August 1974.

NIM reports

The following reports are available free of charge from the National Institute for Metallurgy, Private Bag 7, Auckland Park 2006.

Report No. 1613

Deactivation of copper-activated sphalerite with cyanide.

The rate of deactivation of copper-activated sphalerite with cyanide has been shown to depend on the concentration of free cyanide and on the amount of $Zn(OH)_2$ precipitate present. At concentrations of free cyanide above about 10^{-4}M in the presence of Zn^{2+}, the deactivation is inhibited to a small extent.

The presence of S^{2-}, SO_3^{2-}, or Ca^{2+} has no effect on the rate of deactivation, although it is decreased by the addition of Fe^{2+} and Fe^{3+} (in the form of the respective cyanide).

The results obtained indicate that copper-activated sphalerite, in its reactions with cyanide, does not resemble any of the simple copper sulphides.

Report No. 1639

The determination, by 14 MeV neutron-activation analysis, of small amounts of oxygen and silicon in diamond.

Techniques for the measurement of low levels of oxygen and silicon by fast-neutron-activation analysis have been developed and applied to high-quality diamonds. For oxygen, limits of detection of approximately 5 μg have been established. Sources of error have been studied and eliminated, the ubiquitous occurrence of oxygen being the major problem. Within the accuracy of this work, the results obtained show no significant differences between the oxygen contents of diamonds of different types, or of diamonds from different sources. An oxygen content of 35 ± 4 p.p.m. has been established for high-quality, colourless diamonds. For silicon, a limit of detection of 25 μg was established, and the average silicon content of high-purity diamonds was found to be less than 3 p.p.m. It is concluded that the oxygen in high-purity diamonds is present as CO_2 or H_2O and not in silicate inclusions.

Report No. 1649

The establishment of preferred values for a series of fluorspar samples.

This report correlates the analytical data supplied by fifteen different laboratories for five samples of fluorspar. The results, their statistical treatment, and brief descriptions of the analytical methods used are given. Recommended mean values are assigned to the five samples. Useful results for the minor and trace elements are also included.

Report No. 1668

An updated summary of the world's fluorspar industry.

The world's consumption of fluorspar is expected to increase from 4,7 million tonnes in 1972 to approximately 6,0 million tonnes in 1975, and to 7,3 million tonnes in 1980. Steelmaking accounts for 56 per cent, the balance being consumed in order of importance, by the following industries: aluminium, fluorocarbon, uranium enrichment, stainless-steel pickling, and petroleum alkylation.

South Africa has the largest proven ore reserves (118 million tonnes containing approximately 30 million tonnes of CaF_2) but at present produces only 210 324 tonnes of all grades. However, local producers have realized the future importance of fluorspar and are aware of the indication that South Africa may become the main supplier to the western world from the middle of the next decade.

New plants and extensions to existing plants will probably increase the present capacity from 175 000 tonnes to 410 000 tonnes by 1976. Of this production, 25 per cent may be further processed to agglomerates to be exported as a substitute for metallurgical-grade fluorspar.

Papers of interest

The following papers may be of interest to members.

Surge propagation and reflection on a 400 kV transmission line, by F. G. Heymann

A digital accelerator for torque speed studies, by C. G. Yamey and P. B. Robinson
Trans. S. Afr. Inst. Elec. Engrs, September 1974.

The John Orr Memorial Lecture: Mechanics, pure and simple (applied and elaborated in design), by K. H. Hunt.
S. Afr. Mech. Engr, September 1974.